M Vrigkas, C Nikou, and LP Kondi; "Robust maximum a posteriori image super-resolution," Journal of Electronic Imaging, 23(4), 043016 (2014). doi:10.1117/1.JEI.23.4.043016.

Robust MAP Image Super-Resolution

Michalis Vrigkas,[a] Christophoros Nikou,[a] Lisimachos P. Kondi,[a]
[a]University of Ioannina, Department of Computer Science & Engineering, Ioannina, Greece, 45110

Abstract. A global robust M-estimation scheme for maximum a posteriori (MAP) image super-resolution, which efficiently addresses the presence of outliers in the low resolution images is proposed in this work. In iterative MAP image super-resolution, the objective function to be minimized involves the highly resolved image, a parameter controlling the step size of the iterative algorithm and a parameter weighing the data fidelity term with respect to the smoothness term. Apart from the robust estimation of the high resolution image, the contribution of the proposed method is twofold: (i) the robust computation of the regularization parameters controlling the relative strength of the prior with respect to the data fidelity term and (ii) the robust estimation of the optimal step size in the update of the high resolution image. Experimental results demonstrate that integrating these estimations into a robust framework leads to significant improvement in the accuracy of the high resolution image.

Keywords: Maximum *a posteriori* (MAP) image super-resolution, robust M-estimator, Tikhonov regularization.

Address all correspondence to: Michalis Vrigkas, University of Ioannina, Department of Computer Science & Engineering, Ioannina, Greece, 45110; Tel: +30 265 100 8915; Fax: +30 265 100 8880; E-mail: mvrigkas@cs.uoi.gr

1 Introduction

Image super-resolution (SR) is a technique for enhancing the quality and the resolution of an image. The objective is to improve the spatial resolution by using information from a set of several different low-resolution (LR) images to produce an image with more visible detail in the high spatial frequency features. The LR images may experience different degradations such as motion, point spread function blurring, subsampling and additive noise. The reconstructed high-resolution (HR) image can be successfully estimated if there exist sub-pixel shifts between the LR images. In this manner, each frame of the LR sequence brings complementary information to the original HR image.

Researchers studying the direct inverse solution recognized the limitations of the problem, which is ill-posed due to interpolation, motion compensation, inverse filtering and additive noise.[1–3] Even in cases of perfect motion registration and accurate knowledge of the point spread function

of the acquisition system, a significant dependence of the estimation of the HR image on degradation conditions is observed. A large family of SR methods is based on a stochastic formulation of the problem, which imposes a prior distribution on the image to be reconstructed and provides estimates in a maximum *a posteriori* (MAP) framework, where the posterior distribution of the HR image is maximized.[1–9] In the same context, Bayesian approaches have also been proposed in the literature.[7,10–14]

More recent approaches have shown great potential in recognizing a human face by applying super-resolution techniques. The work of Biligazyev *et al.*[15] recognizes human faces by learning the high-frequency components of facial images and applying them to the LR images in order to create a HR image. Baker and Kanade[16] learn a prior on the spatial distribution of facial images in order to produce a HR image. A Bayesian approach for image super-resolution from a single image is proposed by Tappen and Liu.[17] This method is an alignment based approach that leverages facial low-resolution images. A novel approach which model super-resolved faces in 3D space is presented by Berretti *et al.*[18] 3D scans of low-resolution images are aligned in order to produce a HR 3D face model called "superface".

Violations of the assumptions of data fidelity to the assumed model are also likely to occur, because SR methods are very sensitive to inaccuracies of their parameters. However, little has been reported about suppressing the outliers artifacts (i.e., salt and pepper noise, misregistration errors and occlusion). For instance, median filters have been efficiently used to treat the SR problem[19] where robustness is introduced by applying a median filter in each term of back-projected difference image.

In the same context, a robust color image super-resolution algorithm has previously shown great potential for estimating high-resolution images with crisp details.[20–22] A comparative study

of M-estimators for image super-resolution was presented by El-Yamany and Papamichalis.[20] The main concern of this study is to provide a comparison of the trade off between the estimator robustness and the edge preservation of the high-resolved image. In a preliminary work a robust image super-resolution estimation was introduced. The use of L_1 error norm in the objective function provides a good framework for removing the outliers from the low-resolution images. The work of El-Yamany and Papamichalis[22] introduced a robust error norm in the objective function. The iterative reconstruction process is repeated for every low-resolution image suppressing the outliers without the use of regularization term in the objective function. An independent effort on reducing the aliasing artifacts in a multiframe super-resolution framework using deblurring algorithms is proposed by Robinson *et al.*[23]

Much research has focused on stochastic techniques in a MAP framework.[24,25] Patanavijit *et al.*,[25] used a Huber error norm for measuring the difference between the estimation of HR image and each LR image. A factor that affects the super-resolution quality is also the Tikhonov regularization term, which is used to remove artifacts from the final solutions. Based on a stochastic Bayesian approach, the work of Patanvijit *et al.*[24] performs image super-resolution by minimizing a cost function. The Lorentzian error norm is utilized in order to measure the difference between the estimated high-resolution image (projected onto the low-resolution grid) and each low-resolution image. The authors combine the Tikhonov and the Lorentzian error norms together and use it as regularizer to remove artifacts from the final solution and improve the convergence rate.

The work of Tanaka *et al.*[26] addresses the problem of estimating a high-resolution image in a robust framework. The authors provide an accurate algorithm for extracting single-motion regions and their registration parameters, whereas the whole algorithm is executed in three steps. In the first step, the algorithm estimates the motion parameters between the low-resolution images and

the reference (current high-resolution estimation) image. Then, the region associated with the registration parameters is extracted and finally, the algorithm defines the registration parameters inside the motion region.

Robust image super-resolution algorithms are usually sensitive to their assumed model of data and noise. The work of Farsiu *et al.*[27] introduces a L_1 norm minimization approach for robust image super-resolution using a bilateral prior as a regularizer in order to deal with different data and noise models. This approach preserves the edges of the high-resolved image whereas, it is fast and prone to motion errors, blur and outliers.

The main contribution of this work is the employment of a fully robust image super-resolution technique combined with a MAP framework. The objective function to be minimized employs a regularization term, which controls the smoothness of the reconstructed high-resolved image. The regularization parameters and the optimal step size of the update equation are computed using robust M-estimators in contrast to previous works,[22,24] which employ robust M-estimators only in the estimation of the high-resolution image. Both the regularization parameters and the optimal step size are computed in a closed form from the input data providing thus, more robustness to the estimation of the high-resolved image by retaining crisp details and fully removing the outliers. The proposed method can efficiently reconstruct a high-resolution image from several low-resolution images which suffer from salt and pepper noise, speckle noise, large misregistration errors and occlusion. A four page summary of this work was presented by Vrigkas *et al.*[28] Experiments show that the reconstructed HR image is of higher quality than in standard MAP-based methods[22,24] employing robust estimation only for the estimation of the high-resolution image.

2 Image formation model

The image degradation process[3] is modeled by motion (rotation and translation), a linear blur, and subsampling by pixel averaging along with additive Gaussian noise. We assume that p LR images, each of size $M = N_1 \times N_2$, are obtained from the acquisition process. The following observation model is assumed, where all images are ordered lexicographically

$$\mathbf{y} = \mathbf{W}\mathbf{z} + \mathbf{n}. \tag{1}$$

The set of LR frames is described as $\mathbf{y} = [\mathbf{y}_1^T, \mathbf{y}_2^T, \ldots, \mathbf{y}_p^T]^T$, where $\mathbf{y}_k$, for $k = 1, ...p$, are the p LR images. The desired HR image $\mathbf{z}$ is of size $N = l_1 N_1 \times l_2 N_2$, where l_1 and l_2 represent the up-sampling factors in the horizontal and vertical directions, respectively. The term $\mathbf{n}$ represents zero-mean additive Gaussian noise. In eq. (1), the degradation matrix $\mathbf{W} = [\mathbf{W}_1^T, \mathbf{W}_2^T, \ldots, \mathbf{W}_p^T]^T$ performs the operations of motion, blur and subsampling. Thus, matrix $\mathbf{W}_k$, for the k-th frame, may be written as

$$\mathbf{W}_k = \mathbf{D}\mathbf{B}_k\mathbf{M}(\mathbf{s}_k), \tag{2}$$

where $\mathbf{D}$ is the $N_1 N_2 \times N$ subsampling matrix, $\mathbf{B}_k$ is the $N \times N$ blurring matrix, and $\mathbf{M}(\mathbf{s}_k)$ is the $N \times N$ rigid transformation matrix with parameters (rotation angle and translation vector) denoted by $\mathbf{s}_k$ for the k-th frame. Finally, $\mathbf{n}$ is additive Gaussian noise.

A regularized approach using the image prior information of the HR image (Gaussian assumption) can be used to make the inverse problem well-posed. Considering that each LR image may result from a different degradation process, which implies that different weighting should be given

to it in the desired solution, the following channel-weighted cost function is proposed:[2]

$$L(\mathbf{z}, \mathbf{s}) = \sum_{k=1}^{p} ||\mathbf{y}_k - \mathbf{W}_k(\mathbf{s}_k)\mathbf{z}||^2 + \alpha_k(\mathbf{z})||\mathbf{Q}\mathbf{z}||^2, \tag{3}$$

where $\mathbf{Q}$ is a matrix applying a high pass filter (in our case the Laplacian) and penalizes discontinuities in the final solution. The regularization parameters $\alpha_k(\mathbf{z})$ control the relative contribution between the error term for the k-th LR image (residual norm $||\mathbf{y}_k - \mathbf{W}_k(\mathbf{s}_k)\mathbf{z}||^2$) and the smoothness norm $||\mathbf{Q}\mathbf{z}||^2$. In eq. (3), it is implied that the registration $\mathbf{s}_k$ parameters are collected in $\mathbf{s}$ in this type of formulation.

3 Robust image super-resolution

In our previous work,[2] it has been shown that the regularization parameters $\alpha_k(\mathbf{z})$ may be obtained in closed form from the images:

$$\alpha_k(\mathbf{z}) = \frac{||\mathbf{y}_k - \mathbf{W}_k\mathbf{z}||^2}{2||\mathbf{y}_k||^2 - ||\mathbf{Q}\mathbf{z}||^2}, \tag{4}$$

where we have omitted the dependence of matrix $\mathbf{W}_k$ on the registration parameters $\mathbf{s}_k$ to simplify the notation.

Estimation of the registration parameters $\mathbf{s}$ and the HR image $\mathbf{z}$ may be obtained by an alternating optimization scheme.[1–3] At a first step, the registration parameters may be computed by a variety of methods involving block matching schemes[1–3] or algorithms combining feature extraction and mutual information.[8] Having fixed the registration parameters, we may use a gradient

descent method with a properly calculated step size to minimize (3) with respect to the HR image:

$$\begin{aligned}\hat{\mathbf{z}}^{n+1} &= \hat{\mathbf{z}}^{n} - \varepsilon^{n} g(\hat{\mathbf{z}})^{n}, \\ \hat{\mathbf{z}}^{n+1} &= \hat{\mathbf{z}}^{n} - \sum_{k=1}^{p} \varepsilon_{k}^{n} \mathbf{W}_{k}^{T}(\mathbf{W}_{k}\hat{\mathbf{z}}^{n} - \mathbf{y}_{k}) + \alpha_{k}(\mathbf{z})||\mathbf{Q}\mathbf{z}||^{2}.\end{aligned} \tag{5}$$

The parameter ε^n is the step size at the n-th iteration which may be obtained in closed form directly from the image data[1] by:

$$\varepsilon_{k}^{n} = \frac{\sum_{m=1}^{pM} [\mathbf{W}\mathbf{g}]_{m} [(\mathbf{W}_{k}\mathbf{z} - \mathbf{y}_{k})]_{m} + \sum_{k=1}^{p} \alpha_{k}(\mathbf{z}) \sum_{i=1}^{N} [\mathbf{Q}\mathbf{g}(\mathbf{z})]_{i} [\mathbf{Q}\mathbf{z}]_{i}}{\sum_{m=1}^{pM} [\mathbf{W}\mathbf{g}]_{m}^{2} [(\mathbf{W}_{k}\mathbf{z} - \mathbf{y}_{k})]_{m}^{2} + \sum_{k=1}^{p} \alpha_{k}(\mathbf{z}) \sum_{i=1}^{N} [\mathbf{Q}\mathbf{g}(\mathbf{z})]_{i}}, \tag{6}$$

where the operator $[\cdot]_i$ takes the i-th element of the vectorized matrix inside the brackets.

Super-resolution reconstruction is an ill-posed inverse problem due to the existence of the additive noise. In order to stabilize the inversion process in cases of non Gaussian noise, we introduce a super-resolution algorithm that uses robust error norm in the data fidelity term of the objective function. This approach is based on the class of robust M-estimators. The objective function uses a regularization term that can help the super-resolution algorithm to remove any artifacts from the final solution. We are interested in estimators whose influence function is differentiable and bounded, like the Lorentzian estimator, defined as:

$$\begin{aligned}\rho(x, \sigma) &= \log\left(1 + \tfrac{1}{2}\left(\tfrac{x}{\sigma}\right)^{2}\right), \\ \psi(x, \sigma) &= \tfrac{2x}{2\sigma^{2} + x^{2}},\end{aligned} \tag{7}$$

where σ is the scale factor and ψ is the influence function, defined as the first derivative of the

robust estimator ρ.

The scale factor controls a threshold beyond which all points are considered to be outliers. Violations in the mathematical model in (1) and consequently in the data term in (3) may yield large errors which can severely influence the reconstruction process. The choice of the scale factor σ plays a crucial role in controlling the outliers. Errors falling beyond that threshold are assigned smaller weights and the corresponding outlying measures are suppressed. For small values of the scale factor, the influence function decreases faster assigning smaller weights to errors that outstrip the value of this parameter. If the value of σ is relatively small the contribution of the LR frames will be canceled leading to bad estimation of the HR image, due to the insufficient information provided by the LR frames. On the other hand, if the value of the scale factor is chosen to be arbitrary large, outliers will significantly contribute to the estimation of the HR image. El-Yamani and Papamichalis[22] have presented a method for calculating the outlier threshold, which is based on the similarity between a reference LR frame and the k-th motion-compensated LR frame.

Formulating the observation model of (1) in a M-estimation framework the solution for the HR image is obtained by the following minimization problem:

$$\mathbf{z}^* = \arg\min_{\mathbf{z}} \left\{ \sum_{i=1}^{M} \left[\rho \left(\mathbf{W}_k \mathbf{z} - \mathbf{y}_k; \sigma_k \right) \right]_i + \alpha_k(\mathbf{z}) ||\mathbf{Q}\mathbf{z}||^2 \right\}. \tag{8}$$

Note that in (8), different outlier thresholds are assigned to different LR frames.

Following the calculation of the regularization term in (4), the robust regularization parameter, determining the trade-off between the fidelity of the observed data and the image prior now

becomes:

$$\alpha_k(\mathbf{z}) = \frac{\sum_{i=1}^{M} \left[\rho\left(\mathbf{y}_k - \mathbf{W}_k\mathbf{z};\ \sigma_k\right)\right]_i^2}{2||\mathbf{y}_k||^2 - ||\mathbf{Q}\mathbf{z}||^2}. \tag{9}$$

To obtain a robust solution of (8), the gradient descent scheme of (6) is transformed to its robust counterpart:

$$\hat{\mathbf{z}}^{n+1} = \hat{\mathbf{z}}^n - \sum_{k=1}^{p} \varepsilon_k^n \mathbf{W}_k^T \psi\left(\mathbf{W}_k\hat{\mathbf{z}}^n - \mathbf{y}_k;\ \sigma_k\right) + \alpha_k(\mathbf{z})||\mathbf{Q}\mathbf{z}||^2, \tag{10}$$

where the influence function ψ of the robust estimation is now involved.

It must be noted that the choice of the step-size parameter ε_k^n plays an important role in the behavior of the gradient descent method. This parameter must be small enough to prevent divergence and large enough to provide fast convergence. A constant step-size could be the easiest solution but this is an inappropriate approach for the most of the robust image super-resolution problems. After some manipulation, following the spirit of the approach,[1] a robust closed form solution of the optimal step size may be obtained:

$$\varepsilon_k^n = \frac{\sum_{m=1}^{pM} \left[\mathbf{W}\mathbf{g}\right]_m \left[\psi\left(\mathbf{W}_k\mathbf{z} - \mathbf{y}_k;\ \sigma_k\right)\right]_m + \sum_{k=1}^{p} \alpha_k(\mathbf{z}) \sum_{i=1}^{N} \left[\mathbf{Q}\mathbf{g}(\mathbf{z})\right]_i \left[\mathbf{Q}\mathbf{z}\right]_i}{\sum_{m=1}^{pM} \left[\mathbf{W}\mathbf{g}\right]_m^2 \left[\rho\left(\mathbf{W}_k\mathbf{z} - \mathbf{y}_k;\ \sigma_k\right)\right]_m^2 + \sum_{k=1}^{p} \alpha_k(\mathbf{z}) \sum_{i=1}^{N} \left[\mathbf{Q}\mathbf{g}(\mathbf{z})\right]_i}. \tag{11}$$

Note that both the robust estimator ρ and its influence function ψ appear in (11).

This optimal step size (11) is calculated for every single LR image. Having an adaptive step size, provides a better convergence and also keeps off the algorithm from trapping into erroneous solutions.

In robust image super-resolution reconstruction, it is necessary to define a process for automat-

ically computing the value of the outlier threshold parameter. In statistics, the Median Absolute Deviation (MAD) criterion[29] is considered to be one of the most accurate robust measures of the variability of a univariate sample of quantitative data. For the k-th LR image:

$$\mathrm{MAD}_{\mathrm{k}}^{\mathrm{n}} = \underset{\mathrm{i}}{\mathrm{median}} \left\{ |\mathrm{r}_{\mathrm{k,i}}^{\mathrm{n}}([\mathbf{W}_{\mathrm{k}}\mathbf{z}^{\mathrm{n-1}}; \mathbf{y}_{\mathrm{k}}]_{\mathrm{i}}) - \underset{\mathrm{j}}{\mathrm{median}}(\mathrm{r}_{\mathrm{m,j}}^{\mathrm{n}}([\mathbf{W}_{\mathrm{m}}\mathbf{z}^{\mathrm{n-1}}; \mathbf{y}_{\mathrm{m}})]_{\mathrm{j}})| \right\}, \tag{12}$$

where $n = 0, 1, 2, \ldots$ refers to the n-th iteration of the algorithm and

$$r_{k,i}^{n}(\mathbf{W}_k\mathbf{z}^{n-1}; \mathbf{y}_k) = [\mathbf{W}_k\mathbf{z}^{n-1} - \mathbf{y}_k]_i, \tag{13}$$

is the residual error of the i-th datum between the estimation of the degraded HR image and the k-th LR frame. The MAD is a measure of statistical dispersion. It is a robust statistic, being more resilient to outliers in a data set. In order to use MAD criterion as a consistent estimator for the estimation of the scale factor, we consider $\sigma_k^n = K \cdot \mathrm{MAD}_{\mathrm{k}}^{\mathrm{n}}$, where K is a constant which depends on the distribution. For normally distributed data with standard deviation 1, $K = 1/\Phi^{-1}(3/4) \approx 1.4826$, where Φ^{-1} is the inverse of the cumulative distribution function for the standard normal distribution.[29] In that case, for the k-th LR frame the scale factor σ_k is computed as follows:

$$\sigma_k^n = 1.4826 \cdot \mathrm{MAD}_{\mathrm{k}}^{\mathrm{n}}, \quad \mathrm{k} = 1, 2, \cdots, \mathrm{p}. \tag{14}$$

The scale factor σ_k^n is obtained in an automatic way according to (14) from all the LR frames. In general, the estimation of σ_k^n depends on the similarity between the k-th LR frame and the degraded estimation of the HR image at the n-th iteration. Thus, the scale factor is computed as the median of the residuals. The overall algorithm is summarized in Algorithm 1.

Algorithm 1 Robust super-resolution image reconstruction algorithm.

Input: Low-Resolution images $\mathbf{y}_k, k = 1, 2, \cdots, p$.
Output: High-Resolution image estimate $\hat{\mathbf{z}}^n$.

- First estimate of the HR image $\hat{\mathbf{z}}^0$ using (10).
- Initial estimate of scale factor σ_k^0 with the median of the residual errors for $k = 1, 2, \cdots, p$.
- Register the upscaled $\mathbf{y}_k$ to $\hat{\mathbf{z}}^0, k = 1, 2, \cdots, p$;[8] $n := 1$;
- **do**
  - **do**
    - Random selection of a LR image $\mathbf{y}_k$.
    - **if** $\mathbf{y}_k$ is visited
      - Compute the robust regularization parameter $\alpha_k(\hat{\mathbf{z}}^n)$ using (9).
      - Estimate the optimal step size ε_k^n according to (11).
      - Compute scale factor σ_k^n given in (14).
      - Update $\hat{\mathbf{z}}^n$ using (10).
    - **end**
    - Declare $\mathbf{y}_k$ visited.
  - **until all** $\mathbf{y}_k$ are visited.
  - $n := n + 1$;
  - Declare all $\mathbf{y}_k$, $k = 1, ...p$ unvisited.
- **until** $\|\hat{\mathbf{z}}^{n+1} - \hat{\mathbf{z}}^n\| / \|\hat{\mathbf{z}}^n\| < \epsilon$ or a predefined number of iterations is reached.

Following a similar approach, El-Yamany and Papamichalis[22] introduced the Lorentzian estimator (7) to minimize the objective function and estimate the HR image. They developed a heuristic way of computing the scale factor as a function of the ground truth image and the estimated highly resolved image. Moreover, their step size was defined to be the half of the scale factor value. The Tikhonov regularization has also been used in order to obtain a fine solution for the three channels of color.

The Lorentzian M-estimator is a very popular estimator amongst image reconstruction techniques. The work of Patanavijit *et al.*[24] combines the Lorentzian estimator with a Laplacian

regularization function in order to find a solution to the problem of super-resolution. In their work, the choice of the scale factor, the step size and the regularization parameter is heuristic.

4 Experimental results

In order to evaluate the proposed methodology, four different sets of experiments were conducted on synthetic data sets. Sequences of low resolution images were created by blurring, downsampling and degrading by noise an original image. At first, the images were downsampled by a factor of 2 (4 pixels to 1). Then, a point spread function of a 5×5 Gaussian kernel with standard deviation of 1 was applied and the resulting images were degraded by white Gaussian noise in order to obtain a signal to noise ratio of 30 dB.

To highlight the importance of the proposed fully robust super-resolution scheme we compared it to approaches that employ a robust estimator only in the HR image update and integrate a heuristic scheme for the step size.[22,24] We also compared several robust estimators in that framework: the truncated least squares (TLS), the Geman-McClure and the Lorentzian error norms.

In all experiments, in order to have a first estimate of the HR image, a LR image was chosen at random and it was upscaled by bicubic interpolation. Convergence of the super-resolution algorithm was achieved when $\|\hat{\mathbf{z}}^{n+1} - \hat{\mathbf{z}}^{n}\|/\|\hat{\mathbf{z}}^{n}\| < 10^{-5}$ or until 20 iterations were reached. The convergence of the iterative algorithm is guaranteed by the *contraction mapping theorem*.[30] According to this theorem, the iterative model (5) converges to a unique solution $\hat{\mathbf{z}}$. Therefore, our algorithm always converges.

A quantitative evaluation of the obtained HR images is given by the peak signal to noise ratio (PSNR) defined by:

$$\text{PSNR} = 10 \log_{10} \frac{255^2}{||\mathbf{z} - \hat{\mathbf{z}}||^2}, \tag{15}$$

where $\hat{\mathbf{z}}$ is the estimated HR image and $\mathbf{z}$ is the ground truth.

The structural similarity measure index (SSIM)[31] is a metric that represents a visual distortion between a reference image and the observe LR image. The SSIM is regarded as a function between two images $\mathbf{z}$ and $\hat{\mathbf{z}}$ and it is expressed as:

$$\text{SSIM}(\mathbf{z}, \hat{\mathbf{z}}) = \frac{(2\mu_{\mathbf{z}}\mu_{\hat{\mathbf{z}}} + C_1)(2\sigma_{\mathbf{z}\hat{\mathbf{z}}} + C_2)}{(\mu_{\mathbf{z}}^2 + \mu_{\hat{\mathbf{z}}}^2 + C_1)(\sigma_{\mathbf{z}}^2 + \sigma_{\hat{\mathbf{z}}}^2 + C_2)}, \tag{16}$$

where $\mu_{\mathbf{z}}$ and $\mu_{\hat{\mathbf{z}}}$ denotes the mean intensity of the ground truth and the estimated HR image, respectively. $\sigma_{\mathbf{z}}$ and $\sigma_{\hat{\mathbf{z}}}$ are the standard deviations of the two images and C_1 and C_2 are constants added to avoid instability.

Finally, we have further used the visual information fidelity measure (VIF)[32] in order to assess the quality of the estimated HR image. It is a measure of statistical modeling that could ideally be extracted by the eyebrain system from non-overlapping blocks in a wavelet subband in the high-resolution and the reference images.

(a) (b) (c) (d)

Fig 1 Representative frames of low-resolution images for (a) *Susie*, (b) *Claire*, (c) *Helmet* and (d) *Clock* sequences.

In the first set of experiments, 20 frames of the *Susie* sequence (Figure 1(a)) were used and 50% of them were degraded by salt and pepper noise. Two cases were examined: corruption of 5% and 10% of the pixels in the respective frame. Figures 2(a) and 3(a) depict the reconstructed HR images of the fully robust image super-resolution algorithm for this experiment using three

different types of M-estimators (e.g., Lorentzian, Geman-McClure and TLS) with 5% and 10% salt & pepper noise respectively. In Figures 2(b) and 3(b) the reconstructed HR images with a robust estimator employed only into the estimation of the HR image and not for the parameters ε_k^n and $\alpha_k(\mathbf{z})$ are shown.

Fig 2 Reconstructed high-resolution images for 20 frames of the *Susie* sequence, with salt & pepper noise at 5%. (a) Robust parameters ε_k and $\alpha_k(\mathbf{z})$ and (b) no robust parameters.

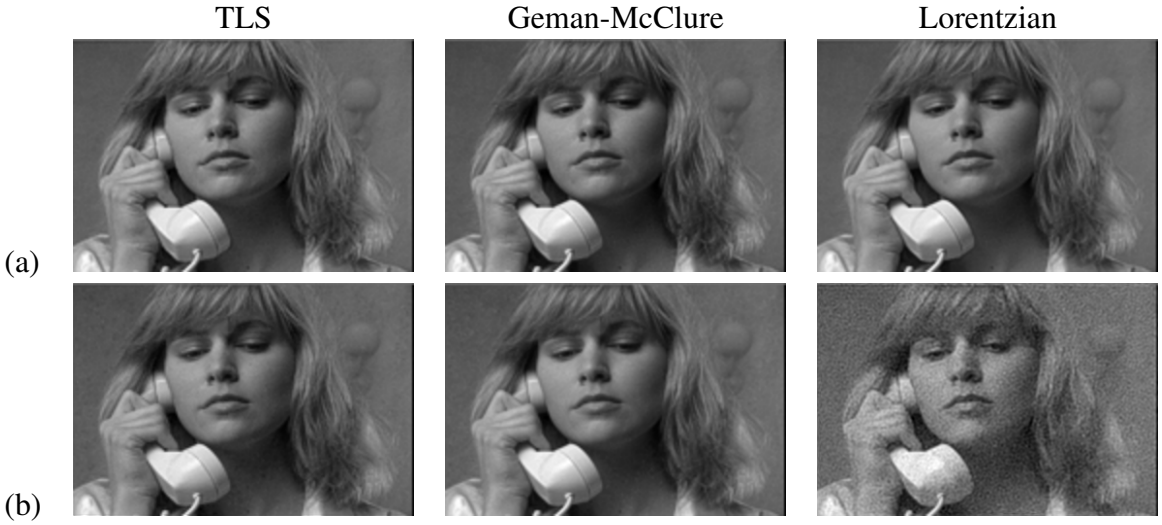

Fig 3 Reconstructed high-resolution images for 20 frames of the *Susie* sequence, with salt & pepper noise at 10%. (a) Robust parameters ε_k and $\alpha_k(\mathbf{z})$ and (b) no robust parameters.

Table 1 presents the statistics of the PSNR for the proposed algorithm for 10 realizations of the

experiment in each case. In this table, the term "partially-robust" refers to the employment of a robust estimator only for the computation of the HR image using (10) but not for the parameters $\alpha_k(\mathbf{z})$ and ε_k^n, which were computed by (4) and (6), respectively. The term term "fully-robust" indicates that a robust estimator was also employed for the computation of $\alpha_k(\mathbf{z})$ and ε_k^n, which were computed using (9) and (11), respectively. The PSNR values in bold indicate the best reconstructed HR image with respect to the robust estimator. In terms of PSNR, the proposed method achieves better reconstruction results with respect to the partially-robust technique and the methods of El-Yamany and Papamichalis[22] and Patanavijit *et al.*[24] for all three robust M-estimators.

Table 2 shows the statistics using the SSIM index. Notice that, the best performance is accomplished for the fully-robust method. In Table 3, the VIF statistics for the *Susie* sequence are shown. As it can be seen, our method achieves better results for the TLS and the Geman-McClure estimator for 5% salt & pepper noise, while it is better than the other methods for 10% salt & pepper noise, when the Lorentzian estimator is employed. The values in bold indicate the best reconstruction result with respect to the robust estimator. Notice that, the TLS estimator underperforms when used with the methods of El-Yamany and Papamichalis[22] and Patanavijit *et. al.*[24]

In the second set of experiments, 20 frames of the *Claire* sequence (Figure 1(b)) were used from which 50% were degraded by speckle noise. Speckle noise is a granular noise which downgrades the quality of an image. Let x_k be the image to which we want to add speckle noise then:

$$y_k = x_k + n \times x_k, \tag{17}$$

where n is uniformly distributed random noise with zero mean and standard deviation σ_2 and y_k is the degraded low-resolution image. Experiments have been conducted for 1% and 2% config-

Table 1 Performance evaluation of the compared robust image super-resolution methods with respect to the PSNR (in *d*B) for the reconstructed image *Susie*, with salt & pepper noise at 5% and 10%.

	Salt & Pepper at 5%											
	method in[22]			method in[24]			partially-robust			fully-robust		
M-Estimator	mean	std	med	mean	std	med	mean	std	med	mean	std	med
Lorentzian	22.1	0.4	22.2	25.2	0.2	25.3	26.6	0.5	26.8	**27.2**	0.5	26.9
TLS	11.1	0.4	10.9	13.9	0.1	13.8	22.3	0.6	22.4	**26.7**	0.3	26.8
Geman	21.4	0.8	22.1	22.0	0.1	22.0	25.6	0.7	25.4	**26.6**	0.1	26.5
	Salt & Pepper at 10%											
	method in[22]			method in[24]			partially-robust			fully-robust		
M-Estimator	mean	std	med	mean	std	med	mean	std	med	mean	std	med
Lorentzian	22.1	0.8	21.9	25.1	0.2	25.0	26.0	0.7	26.3	**26.9**	0.4	26.9
TLS	11.3	0.4	11.0	14.0	0.0	14.0	20.6	0.5	20.7	**25.9**	0.5	26.0
Geman	22.2	0.6	22.0	22.1	0.1	22.1	25.7	0.3	25.8	**25.4**	0.4	25.3

Table 2 Performance evaluation of the compared robust image super-resolution methods with respect to the SSIM statistics for the reconstructed image *Susie*, with salt & pepper noise at 5% and 10%.

	Salt & Pepper at 5%											
	method in[22]			method in[24]			partially-robust			fully-robust		
M-Estimator	mean	std	med	mean	std	med	mean	std	med	mean	std	med
Lorentzian	0.7	0.0	0.7	0.7	0.0	0.7	0.6	0.0	0.6	**0.9**	0.0	0.9
TLS	0.2	0.0	0.2	0.4	0.0	0.4	0.7	0.0	0.7	**0.9**	0.0	0.9
Geman	0.6	0.1	0.6	0.7	0.0	0.7	0.7	0.0	0.7	**0.9**	0.0	0.9
	Salt & Pepper at 10%											
	method in[22]			method in[24]			partially-robust			fully-robust		
M-Estimator	mean	std	med	mean	std	med	mean	std	med	mean	std	med
Lorentzian	0.7	0.0	0.7	0.8	0.0	0.8	0.6	0.0	0.6	**0.9**	0.0	0.9
TLS	0.3	0.0	0.3	0.4	0.0	0.4	0.7	0.1	0.8	**0.9**	0.0	0.9
Geman	0.7	0.0	0.7	0.8	0.0	0.8	0.8	0.0	0.8	**0.9**	0.0	0.9

urations of speckle noise in randomly selected LR image frames. In Figures 4(a) and 5(a) the reconstructed HR images for the *Claire* sequence are shown, with speckle noise at 1% and 2%, using the proposed method. The reconstructed HR images for the same sequence and the same amount of noise using the partially-robust technique are shown in Figures 4(b) and 5(b). As it can

Table 3 Performance evaluation of the compared robust image super-resolution methods with respect to the VIF statistics for the reconstructed image *Susie*, with salt & pepper noise at 5% and 10%.

	Salt & Pepper at 5%											
	method in[22]			method in[24]			partially-robust			fully-robust		
M-Estimator	mean	std	med	mean	std	med	mean	std	med	mean	std	med
Lorentzian	0.6	0.0	0.6	0.8	0.0	0.8	0.5	0.0	0.5	**0.9**	0.0	0.9
TLS	0.1	0.0	0.1	0.1	0.0	0.1	0.8	0.1	0.8	**0.9**	0.0	0.9
Geman	0.1	0.0	0.5	0.8	0.0	0.8	0.8	0.0	0.8	**0.9**	0.0	0.9
	Salt & Pepper at 10%											
	method in[22]			method in[24]			partially-robust			fully-robust		
M-Estimator	mean	std	med	mean	std	med	mean	std	med	mean	std	med
Lorentzian	0.6	0.0	0.5	0.8	0.0	0.8	0.5	0.0	0.5	**0.9**	0.0	0.9
TLS	0.1	0.0	0.1	0.1	0.0	0.1	0.7	0.1	0.7	**0.9**	0.0	0.9
Geman	0.5	0.0	0.5	0.8	0.0	0.8	0.8	0.0	0.8	**0.9**	0.0	0.9

be observed, the fully-robust method is able to fully wipe away speckle noise and reconstruct a clean image while the partially-robust method suffers from noise artifacts.

Fig 4 Reconstructed high-resolution images for 20 frames of the *Claire* sequence, with speckle noise at 1%. (a) Robust parameters ε_k and $\alpha_k(\mathbf{z})$ and (b) no robust parameters.

In Table 4, the PSNR values for the reconstructed *Claire* sequence with speckle noise 1% and 2% are shown. The robust variant is the most accurate SR method for all three M-estimators. Tables

Fig 5 Reconstructed high-resolution images for 20 frames of the *Claire* sequence, with speckle noise at 2%. (a) Robust parameters ε_k and $\alpha_k(\mathbf{z})$ and (b) no robust parameters.

5 and 6 present the SSIM and VIF statistics for the same sequence. As it can be seen, the TLS estimator is does not perform very well when associated with the El-Yamany and Papamichalis[22] and Patanavijit *et al.*[24] methods.

Table 4 Performance evaluation of the compared robust image super-resolution methods with respect to the PSNR (in dB) for the reconstructed image *Claire*, with speckle noise at 1% and 2%.

	Speckle at 1%											
	method in[22]			method in[24]			partially-robust			fully-robust		
M-Estimator	mean	std	med	mean	std	med	mean	std	med	mean	std	med
Lorentzian	22.3	0.5	22.3	27.8	0.1	27.8	23.3	0.4	23.3	**29.9**	0.1	30.5
TLS	10.4	0.3	10.3	11.5	0.1	11.5	16.9	0.6	16.8	**28.2**	0.6	28.3
Geman	21.6	0.8	21.3	23.2	0.16	23.2	29.0	0.4	29.0	**29.8**	0.5	30.0
	Speckle at 2%											
	method in[22]			method in[24]			partially-robust			fully-robust		
M-stimator	mean	std	med	mean	std	med	mean	std	med	mean	std	med
Lorentzian	22.6	0.7	22.7	27.9	0.1	27.9	22.2	0.8	22.6	**31.2**	0.8	31.5
TLS	10.5	0.1	10.5	11.5	0.1	11.5	14.3	0.5	14.0	**29.5**	0.5	29.4
Geman	21.6	0.5	21.5	23.2	0.1	23.1	28.8	0.6	29.4	**31.1**	0.2	31.1

The third set of experiments, contains a sequence of 10 LR frames depicting a football helmet

Table 5 Performance evaluation of the compared robust image super-resolution methods with respect to the SSIM statistics for the reconstructed image *Claire*, with speckle noise at 1% and 2%.

	Speckle at 1%											
	method in[22]			method in[24]			partially-robust			fully-robust		
M-Estimator	mean	std	med	mean	std	med	mean	std	med	mean	std	med
Lorentzian	0.8	0.0	0.8	0.8	0.0	0.8	0.6	0.2	0.6	**0.9**	0.1	0.9
TLS	0.4	0.1	0.4	0.5	0.0	0.5	0.6	0.1	0.7	**0.9**	0.1	0.9
Geman	0.8	0.0	0.8	0.8	0.0	0.8	0.8	0.0	0.8	**0.9**	0.0	0.9
	Speckle at 2%											
	method in[22]			method in[24]			partially-robust			fully-robust		
M-Estimator	mean	std	med	mean	std	med	mean	std	med	mean	std	med
Lorentzian	0.8	0.0	0.8	0.8	0.0	0.8	0.5	0.2	0.5	**0.9**	0.0	0.9
TLS	0.3	0.1	0.4	0.5	0.0	0.5	0.7	0.1	0.7	**0.7**	0.0	0.9
Geman	0.8	0.1	0.7	0.8	0.0	0.8	0.8	0.0	0.8	**0.9**	0.0	0.9

Table 6 Performance evaluation of the compared robust image super-resolution methods with respect to the VIF statistics for the reconstructed image *Claire*, with speckle noise at 1% and 2%.

	Speckle at 1%											
	method in[22]			method in[24]			partially-robust			fully-robust		
M-Estimator	mean	std	med	mean	std	med	mean	std	med	mean	std	med
Lorentzian	0.3	0.0	0.3	0.7	0.0	0.7	0.4	0.1	0.4	**0.8**	0.2	0.8
TLS	0.1	0.0	0.1	0.1	0.0	0.1	0.3	0.1	0.3	**0.7**	0.1	0.7
Geman	0.3	0.2	0.2	0.6	0.0	0.6	0.6	0.0	0.6	**0.7**	0.1	0.8
	Speckle at 2%											
	method in[22]			method in[24]			partially-robust			fully-robust		
M-Estimator	mean	std	med	mean	std	med	mean	std	med	mean	std	med
Lorentzian	0.4	0.0	0.4	0.7	0.0	0.7	0.3	0.1	0.3	**0.8**	0.1	0.8
TLS	0.1	0.0	0.1	0.1	0.0	0.1	0.4	0.2	0.4	**0.7**	0.0	0.7
Geman	0.3	0.0	0.3	0.7	0.0	0.7	0.7	0.0	0.7	**0.8**	0.0	0.8

(Figure 1(c)). In order to simulate motion errors, a global translational model is assumed. 30% of randomly selected LR images were transformed by translation of 15 pixels along the horizontal and vertical directions whereas a rotation of 20 degrees was also applied. The misalignment is large and the standard super-resolution reconstruction methods can not account for it with out a

robust estimator. The reconstructed HR images for the proposed method are depicted in Figure 6(a) and for the partially-robust method are shown in Figure 6(b). As it can be seen, the proposed method can successfully suppress the effect of outliers resulting to an image free of noise artifacts. On the other hand, the partially-robust technique is of sightly lower quality.

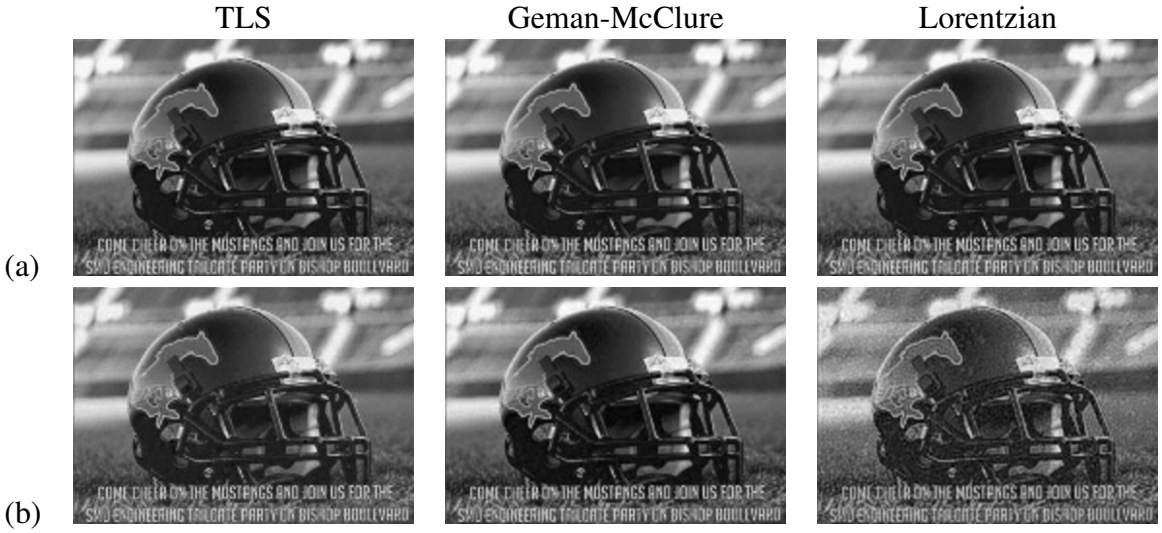

Fig 6 Reconstructed high-resolution images for 20 frames of the *Helmet* sequence. (a) Robust parameters ε_k and $\alpha_k(\mathbf{z})$ and (b) no robust parameters.

Tables 7, 8 and 9 present the PSNR, SSIM index and VIF numerical results respectively for this experiment comparing the proposed fully-robust method against the partially-robust version, and the methods of El-Yamany and Papamichalis[22] and Patanavijit *et. al.*[24] The values in bold indicate the best performance for the corresponding robust estimator. Notice that the proposed method performs better than the other methods in all experiments and the worst performance is achieved by the TLS estimator for all methods.

Finally, the fourth set of experiments, consists of a sequence of seven LR frames (Figure 1(d)). In two out of seven consecutive frames an object appears representing occlusion. Occlusion was intentionally added in order to simulate accidental changes in the scene and it is treated as an outlier by the method. The reconstructed HR images for the proposed method using the three M-

Table 7 Performance evaluation of the compared robust image super-resolution methods with respect to the PSNR (in dB) for the reconstructed image *Helmet*.

	method in[22]			method in[24]			partially-robust			fully-robust		
M-Estimator	mean	std	med	mean	std	med	mean	std	med	mean	std	med
Lorentzian	20.4	0.5	20.4	23.1	0.0	23.1	18.4	0.4	18.9	**23.8**	0.4	23.0
TLS	7.5	0.4	7.3	14.4	0.1	14.4	19.9	0.6	20.0	**23.0**	0.0	23.0
Geman	20.4	0.9	20.5	22.7	0.1	22.7	22.5	0.3	22.5	**23.0**	0.0	23.0

Table 8 Performance evaluation of the compared robust image super-resolution methods with respect to the SSIM statistics for the reconstructed image *Helmet*.

	method in[22]			method in[24]			partially-robust			fully-robust		
M-Estimator	mean	std	med	mean	std	med	mean	std	med	mean	std	med
Lorentzian	0.7	0.0	0.7	0.8	0.0	0.8	0.7	0.1	0.6	**0.9**	0.0	0.9
TLS	0.1	0.0	0.1	0.5	0.0	0.5	0.7	0.1	0.7	**0.8**	0.0	0.8
Geman	0.7	0.0	0.7	0.8	0.0	0.8	0.8	0.0	0.8	**0.9**	0.0	0.9

Table 9 Performance evaluation of the compared robust image super-resolution methods with respect to the VIF statistis for the reconstructed image *Helmet*.

	method in[22]			method in[24]			partially-robust			fully-robust		
M-Estimator	mean	std	med	mean	std	med	mean	std	med	mean	std	med
Lorentzian	0.7	0.0	0.7	0.7	0.0	0.7	0.5	0.1	0.5	**0.8**	0.1	0.8
TLS	0.2	0.0	0.2	0.4	0.0	0.4	0.6	0.1	0.6	**0.7**	0.0	0.7
Geman	0.7	0.1	0.7	0.7	0.0	0.7	0.7	0.0	0.7	**0.8**	0.0	0.8

estimators are illustrated in Figure 7(a). Figure 7(b) depicts the reconstructed HR images when the partially-robust approach is employed. As it can be seen, there is a visible noise distortion in the reconstructed images which is caused by the non robust computation of the parameters ε_k and $\alpha_k(\mathbf{z})$.

The PSNR, SSIM index and VIF statistic results are presented in Tables 10, 11 and 12 respectively. The values in bold represent the best performance for the corresponding robust estimator. Our method performs better in all cases of experiments and is able to fully reconstruct a HR image suppressing the outliers in the cases where partial occlusion is apparent in the low resolution im-

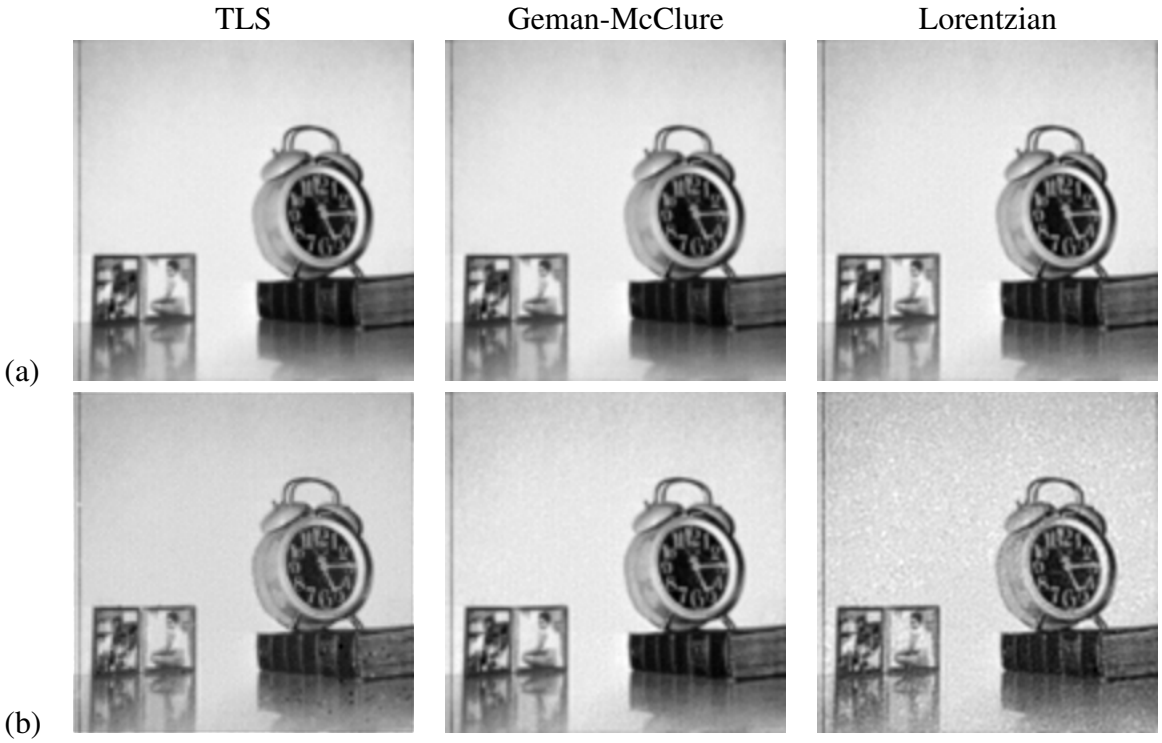

Fig 7 Reconstructed high-resolution images for 20 frames of the *Clock* sequence. (a) Robust parameters ε_k and $\alpha_k(\mathbf{z})$ and (b) no robust parameters.

ages. For the method of El-Yamany and Papamichalis[22] the least good estimator seems to be the Geman-McClure, whereas for the method of Patanavijit *et al.*[24] the least good estimator seems to be the TLS. Let us recall that in all experiments involving the proposed method the parameters ε_k and $\alpha_k(\mathbf{z})$ were robustly estimated and the outlier threshold was computed using the MAD criterion (14) suppressing thus, many outliers, which have been occurred by noise artifacts, misregistration errors or occlusion.

Table 10 Performance evaluation of the compared robust image super-resolution methods with respect to the PSNR (in dB) for the reconstructed image *Clock*.

	method in[22]			method in[24]			partially-robust			fully-robust		
M-Estimator	mean	std	med	mean	std	med	mean	std	med	mean	std	med
Lorentzian	25.1	0.1	25.1	25.1	0.0	25.1	22.0	0.18	22.2	**25.8**	0.1	25.8
TLS	24.1	0.1	24.07	10.1	0.1	10.1	16.8	0.4	16.1	**24.8**	0.2	24.8
Geman	9.8	0.2	9.7	24.7	0.2	24.6	25.1	0.3	25.2	**25.2**	0.1	25.2

Table 11 Performance evaluation of the compared robust image super-resolution methods with respect to the SSIM statistics for the reconstructed image *Clock*.

	method in[22]			method in[24]			partially-robust			fully-robust		
M-Estimator	mean	std	med	mean	std	med	mean	std	med	mean	std	med
Lorentzian	0.8	0.0	0.8	0.8	0.0	0.8	0.7	0.0	0.7	**0.9**	0.0	0.9
TLS	0.8	0.0	0.8	0.7	0.0	0.7	0.7	0.2	0.7	**0.9**	0.0	0.9
Geman	0.5	0.0	0.5	0.8	0.0	0.8	0.8	0.0	0.8	**0.9**	0.0	0.9

Table 12 Performance evaluation of the compared robust image super-resolution methods with respect to the VIF statistics for the reconstructed image *Clock*.

	method in[22]			method in[24]			partially-robust			fully-robust		
M-Estimator	mean	std	med	mean	std	med	mean	std	med	mean	std	med
Lorentzian	0.7	0.0	0.7	0.7	0.0	0.7	0.7	0.0	0.7	**0.9**	0.0	0.9
TLS	0.7	0.0	0.7	0.3	0.0	0.3	0.5	0.2	0.5	**0.8**	0.0	0.8
Geman	0.2	0.0	0.2	0.7	0.0	0.7	0.7	0.0	0.7	**0.8**	0.0	0.8

5 Conclusions

In this paper, we presented a fully robust image super-resolution algorithm, where the estimation of the HR image was integrated in two steps. First, the regularization parameters were robustly estimated in an automatic manner and then, the optimal step size of the update of the high-resolution image was computed for every single LR frame. The outlier threshold was automatically estimated in a robust framework as the residual error between the estimation of the degraded HR image and the upscaled k-th LR frame. We demonstrated that under different assumptions and different M-estimators we can derive a powerful super-resolution algorithm that suppresses the effect of outliers.

References

1 R. C. Hardie, K. J. Barnard, and E. E. Armstrong, "Joint MAP image registration and high-resolution image estimation using a sequence of undersampled images," *IEEE Transactions*

on Image Processing **6**, 1621–1633 (1997).

2 H. He and L. P. Kondi, "Resolution enhancement of video sequences with simultaneous estimation of the regularization parameter," *SPIE Journal of Electronic Imaging* **13**(3), 586–596 (2004).

3 H. He and L. P. Kondi, "An image super-resolution algorithm for different error levels per frame," *IEEE Transactions on Image Processing* **15**, 592–603 (2006).

4 D. Capel and A. Zisserman, "Computer vision applied to super-resolution," *IEEE Signal Processing Magazine* **20**(3), 75–86 (2003).

5 G. K. Chantas, N. P. Galatsanos, and N. A. Woods, "Super-resolution based on fast registration and maximum a posteriori reconstruction," *IEEE Transactions on Image Processing* **16**, 1821–1830 (2007).

6 T. Q. Pham, L. J. van Vliet, and K. Schutte, "Robust super-resolution without regularization," in *Proc.* 4^{th} *AIP International Conference and the 1st Congress of the IPIA, in: Journal of Physics: Conference Series 124*, *012036*, 1–20 (2008).

7 L. C. Pickup, D. P. Capel, S. J. Roberts, and A. Zisserman, "Overcoming registration uncertainty in image super-resolution: maximize or marginalize?," *EURASIP Journal on Advances in Signal Processing* **2007**, 20–20 (2007).

8 M. Vrigkas, C. Nikou, and L. P. Kondi, "On the improvement of image registration for high accuracy super-resolution," in *Proc. IEEE International Conference on Acoustics, Speech and Signal Processing*, 981–984, (Prague, Czech Republic) (2011).

9 F. Šroubek and J. Flusser, "Resolution enhancement via probabilistic deconvolution of multiple degraded images," *Pattern Recognition Letters* **27**(4), 287–293 (2006).

10 S. Farsiu, M. Elad, and P. Milanfar, "Multi-frame demosaicing and super-resolution of color images," *IEEE Transactions on Image Processing* **15**, 141–159 (2006).

11 A. Kanemura, S. Maeda, and S. Ishii, "Edge-preserving Bayesian image superresolution based on compound Markov random fields," in *Proc.* 17^{th} *International conference on Artificial Neural Networks*, 611–620, (Porto, Portugal) (2007).

12 L. C. Pickup, D. P. Capel, S. J. Roberts, and A. Zisserman, "Bayesian image super-resolution, continued," in *Proc. Advances in Neural Information Processing Systems*, 1089–1096, MIT Press (2006).

13 C. A. Segall, A. K. Katsaggelos, R. Molina, and J. Mateos, "Bayesian resolution enhancement of compressed video," *IEEE Transactions on Image Processing* **13**, 898–911 (2004).

14 M. E. Tipping and C. M. Bishop, "Bayesian image super-resolution," in *Proc. Advances in Neural Information Processing Systems*, 1303–1310, MIT Press (2003).

15 E. Bilgazyev, B. A. Efraty, S. K. Shah, and I. A. Kakadiaris, "Improved face recognition using super-resolution," in *Proc. International Joint Conference on Biometrics*, 1–7 (2011).

16 S. Baker and T. Kanade, "H. faces," in 4^{th} *IEEE International Conference on Automatic Face and Gesture Recognition*, 83–89, (Grenoble, France) (2000).

17 M. F. Tappen and C. Liu, "A Bayesian approach to alignment-based image hallucination," in *Proc. European Conference on Computer Vision*, 236–249, (Firenze, Italy) (2012).

18 S. Berretti, A. D. Bimbo, and P. Pala, "Superfaces: A super-resolution model for 3d faces," in *Proc. European Conference on Computer Vision*, 73–82, (Firenze, Italy) (2012).

19 A. Zomet, A. Rav-Acha, and S. Peleg, "Robust super-resolution," in *Proc. IEEE Workshop on Applications of Computer Vision*, **1**, 645–650 (2001).

20 N. A. El-Yamany and P. E. Papamichalis, "Using bounded-influence M-estimators in multi-frame super-resolution reconstruction: a comparative study," in *Proc.* 15^{th} *IEEE International Conference on Image Processing*, 337–340 (2008).

21 N. A. El-Yamany and P. E. Papamichalis, "An adaptive M-estimation framework for robust image superresolution without regularization," *Visual Communications and Image Processing* **6822**, 1–12 (2008).

22 N. A. El-Yamany and P. E. Papamichalis, "Robust color image superresolution: An adaptive M-estimation framework," *EURASIP Journal on Image and Video Processing* (2008). ID=763254.

23 M. D. Robinson, C. A. T. J. Y. Lo, and S. Farsiu, "Efficient fourier-wavelet super-resolution," *IEEE Transactions on Image Processing* **19**(10), 2669–2681 (2010).

24 V. Patanavijit, S. Tae-O-Sot, and S. Jitapunkul, "A Lorentzian stohastic estimation for a robust iterative multiframe supr-resolution reconstruction with Lorentzian-tikhonov regularization," *EURASIP Journal on Advatages in Signal Processing* (2007). ID=34821.

25 V. Patanavijit, S. Tae-O-Sot, and S. Jitapunkul, "A robust iterative superresolution reconstruction of image sequences using a Lorentzian Bayesian approach with fast affine block-based registration," in *Proc. IEEE International Conference on Image Processing*, **5**, 393–396 (2007).

26 M. Tanaka, Y. Yaguchi, and M. Okutomi, "Robust and accurate estimation of multiple motions for whole-image super-resolution," in *Proc. IEEE International Conference on Image Processing*, 649–652, (San Diego, California, USA) (2008).

27 S. Farsiu, M. D. Robinson, M. Elad, and P. Milanfar, "Fast and robust multiframe super resolution," *IEEE Transactions on Image Processing* **13**, 1327–1344 (2004).

28 M. Vrigkas, C. Nikou, and L. P. Kondi, "A fully robust framework for MAP image super-resolution," in *Proc. IEEE International Conference on Image Processing*, 2225–2228, (Orlando, Florida, USA) (2012).

29 P. J. Rousseeuw and A. M. Leory, *Robust Regression and Outlier Detection*, John Wiley & Sons (1987).

30 A. K. Katsaggelos, "Iterative image restoration algorithms," *Optical Engineering* **28**(7), 735–748 (1989).

31 Z. Wang, A. C. Bovik, H. R. Sheikh, and E. P. Simoncelli, "Image quality assessment: from error visibility to structural similarity," *IEEE Transactions on Image Processing* **13**(4), 600–612 (2004).

32 H. R. Sheikh and A. C. Bovik, "Image information and visual quality," *IEEE Transactions on Image Processing* **15**(2), 430–444 (2006).

Michalis Vrigkas received the B.Sc. and M.Sc. in Computer Science from the University of Ioannina, Greece, in 2008 and 2010, respectively. He is currently pursuing the Ph.D. degree in the Department of Computer Science and Engineering, University of Ioannina, Greece. He has participated in several EC-funded ICT projects. His research interests include image processing and analysis, computer vision, machine learning and pattern recognition.

Christophoros Nikou received the Diploma in electrical engineering from the Aristotle University of Thessaloniki, Greece, in 1994 and the DEA and Ph.D. degrees in image processing and computer

vision from Louis Pasteur University, Strasbourg, France, in 1995 and 1999, respectively. He was a Senior Researcher with the Department of Informatics, Aristotle University of Thessaloniki in 2001. From 2002 to 2004, he was a Research Engineer and Project Manager with Compucon S.A., Thessaloniki, Greece. He was a Lecturer (2004-2009) and an Assistant Professor (2009-2013) with the Department of Computer Science and Engineering, University of Ioannina, Ioannina, Greece, where he has been an Assiociate Professor, since 2013. His research interests mainly include image processing and analysis, computer vision and pattern recognition and their application to medical imaging. He is a member of EURASIP and an IEEE Senior Member.

Lisimachos P. Kondi received the Diploma in electrical engineering from the Aristotle University of Thessaloniki, Greece, in 1994 and the M.S. and Ph.D. degrees in electrical and computer engineering from Northwestern University, Evanston, IL, in 1996 and 1999, respectively.

During the 1999-2000 academic year, he was a Postdoctoral Research Associate at Northwestern University. He is currently an Associate Professor with the Department of Computer Science and Engineering, University of Ioannina, Greece. He was previously with the faculty of the University at Buffalo, The State University of New York, and has also held summer appointments at the Naval Research Laboratory, Washington, DC, and the Air Force Research Laboratory, Rome, NY. His research interests are in the general areas of signal and image processing and communications, including image and video compression and transmission over wireless channels and the Internet, sparse models and compressive sensing, super-resolution of video sequences, and shape coding.

Dr. Kondi has been an Associate Editor of the IEEE Signal Processing Letters (2008-2012), the EURASIP Journal on Advances in Signal Processing (2005-present), and the International

Journal of Distributed Sensor Networks (2013-present). He was also Technical Program Chair of the International Conference on Digital Signal Processing (Santorini, Greece, July 2013).